

Low temperature ferromagnetism in $CaCu_3Ti_4O_{12}$

Song Yang(杨松), Xiao-Jing Luo(罗晓婧), Zhi-Ming Shen(申志明), Tian Gao(高湉), Yong-Sheng Liu(刘永生), and Shao-Long Tang(唐少龙)

Citation: Chin. Phys. B, 2021, 30 (**9**): 098103. DOI: 10.1088/1674-1056/abeef0
Journal homepage: http://cpb.iphy.ac.cn; http://iopscience.iop.org/cpb

What follows is a list of articles you may be interested in

Hydrothermal synthesis and characterization of carbon-doped TiO_2 nanoparticles

Zafar Ali, Javaid Ismail, Rafaqat Hussain, A. Shah, Arshad Mahmood, Arbab Mohammad Toufiq, and Shams ur Rahman

Chin. Phys. B, 2020, 29 (**11**): 118102. DOI: 10.1088/1674-1056/ab9f29

A systematic study of light dependency of persistent photoconductivity in a-InGaZnO thin-film transistors

Yalan Wang(王雅兰), Mingxiang Wang(王明湘), Dongli Zhang(张冬利), and Huaisheng Wang(王槐生)

Chin. Phys. B, 2020, 29 (**11**): 118101. DOI: 10.1088/1674-1056/abb222

Positive gate bias stress-induced hump-effect in elevated-metal metal-oxide thin film transistors

Dong-Yu Qi(齐栋宇), Dong-Li Zhang(张冬利), Ming-Xiang Wang(王明湘)

Chin. Phys. B, 2017, 26 (**12**): 128101. DOI: 10.1088/1674-1056/26/12/128101

Bound states of Dirac fermions in monolayer gapped graphene in the presence of local perturbations

Mohsen Yarmohammadi, Malek Zareyan

Chin. Phys. B, 2016, 25 (**6**): 068105. DOI: 10.1088/1674-1056/25/6/068105

Effects of Ni doping on the structural properties and collapse of magnetic ordering in $NdFe_{1}$-xNi_xO_3 ($0.1 \le x \le 0.7$) orthoferrites

I. Ahmad, M. J. Akhtar, M. Siddique

Chin. Phys. B, 2016, 25 (**2**): 028101. DOI: 10.1088/1674-1056/25/2/028101

Low temperature ferromagnetism in $CaCu_3Ti_4O_{12}$*

Song Yang(杨松)[1], Xiao-Jing Luo(罗晓婧)[1,†], Zhi-Ming Shen(申志明)[1], Tian Gao(高淀)[1], Yong-Sheng Liu(刘永生)[1], and Shao-Long Tang(唐少龙)[2,‡]

[1] *Shanghai Key Laboratory of Materials Protection and Advanced Materials in Electric Power, Shanghai* 200090, *China*
[2] *Nanjing National Laboratory of Microstructures, Jiangsu Provincial Laboratory for Nanotechnology and Department of Physics, Nanjing University, Nanjing* 210093, *China*

(Received 31 December 2020; revised manuscript received 14 February 2021; accepted manuscript online 16 March 2021)

The low-temperature magnetic order behaviors of perovskite oxide $CaCu_3Ti_4O_{12}$ (CCTO) ceramics prepared by different methods are discussed. X-ray diffraction, scanning electron microscope, x-ray photoelectron spectroscopy, and direct current (DC) magnetization are used to characterize the structures, microscopic morphologies, valence states, and magnetic properties of the samples. The results show that the magnetic behaviors of CCTO ceramics are very sensitive to the preparation process. The quenched CCTO ceramic and CCTO powders grown in a molten salt crystal, which contain much more oxygen vacancies and Ti^{3+}, show the coexistence of weak ferromagnetic order and antiferromagnetic order below the Neel temperature. It suggests that the bound magnetopolaron formed by oxygen vacancies and Ti^{3+} ion composite defects are responsible for the weak ferromagnetic order at low temperature.

Keywords: $CaCu_3Ti_4O_{12}$, oxygen vacancies, magnetic ordering

PACS: 81.40.Rs **DOI:** 10.1088/1674-1056/abeef0

1. Introduction

The perovskite-type material $CaCu_3Ti_4O_{12}$ (CCTO) has received extensive attention because of its huge dielectric constant (up to 10^5) and the abnormal dielectric properties.[1,2] Many experimental and theoretical studies have tried to clarify its dielectric origin.[3–10] The crystal structure of CCTO is quite stable so that the long-range crystallographic structure can last down to 35 K.[1] Even under the high pressure up to 57 GPa no structural change can be observed by high-resolution x-ray diffraction.[11] However, the dielectric properties are sensitive to the sample preparation process or measurement conditions,[12–15] suggesting an extrinsic dielectric origin which is somewhat related to the defects. Especially, oxygen vacancies play an important role in the conduction and dielectric polarization of CCTO.[16–18] Afterwards, we have to think whether the magnetic properties of CCTO as a member of perovskite transition metal oxide family which usually has rich electric or magnetic physical properties, are affected by oxygen vacancy-related defects. In the study of titanium-based diluted magnetic semiconductor, such as TiO_2, many researchers have demonstrated the contributions of oxygen vacancy defects to the room temperature ferromagnetism.[19–25] Thus, we should think of the similar questions in CCTO. Generally, pure CCTO is antiferromagnetic (AFM) at low temperature with a Neel temperature (T_N) of about 25 K, which has been confirmed by some researchers through neutron scattering, Raman spectroscopy and electron spin resonance.[26–28] However, it is found that the antiferromagnetic phase is not pure, but sometimes there is a Curie tail[28,29] or an indication of ferromagnetic (FM) characteristics[30,31] below Neel temperature, which depend on the doping or sample preparation process. For example, Pires *et al.* found Curie tails below 25 K in the thermomagnetic curves of polycrystalline CCTO annealed under argon atmosphere and the single crystal CCTO samples.[28] They thought that the Curie tails are attributed to the magnetic Ti^{3+}, which is caused by the oxygen vacancies present in both samples. In pure Fe- or Nb-doped CCTO samples, Fernandez *et al*. also found the Curie tails, which could be fitted well by the Curie–Weiss paramagnetic behavior after subtracting the background of the AFM behavior. The authors also thought that the paramagnetic phase is contributed by the Ti^{3+} ions as indicated by the analysis of the x-ray photoelectron spectrum.[29] However, there is no further investigation of magnetic hysteresis loops in the temperature ranges in which the Curie tails appear. Actually, Raval *et al.* also found Curie tails and a weak ferromagnetic loop in pure CCTO polycrystals at 5 K, only by changing the mechanical grinding time in the sample preparation process. They deduced that the ferromagnetic characteristic may be attributed to oxygen vacancies introduced in the mechanical grinding process.[31] The

*Project supported by the National Natural Science Foundation of China (Grant Nos. 11504227 and 51971128), the Program of Shanghai Academic/Technology Research Leader, China (Grant No. 20XD1401800), and the Project of the Science and Technology Commission of Shanghai Municipality, China (Grant No. 19020501000).

†Corresponding author. E-mail: xiaojing_luo@163.com
‡Corresponding author. E-mail: tangsl@nju.edu.cn

© 2021 Chinese Physical Society and IOP Publishing Ltd

FM state was also indeed obtained by doing 5 at.%–7 at.% of Fe[30] or doping 10 at.% of Co ions.[32] These results show that the magnetic properties are also sensitive to the doping or sample preparation process, which may closely relate to oxygen–vacancy-associated defects. In this work, we try to prepare CCTO samples through different sample preparation processes, in order to reveal the relationship between oxygen vacancies and magnetism in CCTO.

2. Experimental details

Polycrystalline $CaCu_3Ti_4O_{12}$ ceramics were synthesized by solid phase reaction method through using analytically pure raw materials of $CaCO_3$ (99.99%), CuO (99.0%), and TiO_2 (99.5%). First, the raw material powders were mixed uniformly with ethanol as a medium in an agate mortar at the stoichiometric ratio, and pre-sintered for 10 h at 900 °C. Then, the pre-sintered powders were pressed into disks, and the disks were pre-sintered at 1000 °C for 10 h again. After that, the pre-sintered pellets were reground and pressed into disks, and then the disks were sintered at 1100 °C for 24 hours in air. Finally, dense ceramics were obtained and named as-sintered ceramic. In order to obtain different sample conditions, some sintered disks were reground and pellted, and then quenched at 800 °C for 10 min in a high-pressure component of 6 GPa, and then dense ceramics were obtained and called the quenched ceramic. For comparison, the quenched ceramics were annealed at 600 °C for 20 h in air and referred to as annealed ceramic. We also prepared the CCTO powders by a molten salt method. Specifically, $CaCO_3$ (99.99%), CuO (99.0%), and TiO_2 (99.5%) were used as raw materials, and Na_2SO_4 (99.0%), and K_2SO_4 (99.0%) served as molten salt additives. The raw materials were mixed with salt additives and sintered at 950 °C for 5 h. After that the salt was removed by the dissolution in hot deionized water, with CCTO powders left and dried and termed CCTO-M.

The structural characterization was carried out with x-ray powder diffraction (XRD, Bruker D8 Advance, and Cu $K\alpha$) at room temperature (300 K). The microscopic morphologies of the samples were characterized by a cold field emission scanning electron microscope (SEM, Hitachi S4800K). X-ray photoelectron spectroscopy (XPS Thermo ESCALAB 250XI) was used to estimate the valence state of ions and identify the defects in the samples. The magnetic properties of the samples were examined by employing the vibrating sample magnetometer (VSM) on a physical property measurement system (PPMS-9, Quantum Design Inc., USA). A 20-Oe (1 Oe = 79.5775 $A{\cdot}m^{-1}$) magnetic field was used in the field cooling (FC) mode and the zerofield cooling (ZFC) mode, and the thermomagnetic (M–T) curve in a temperature range of 3 K–300 K was recorded.

3. Results and discussion

3.1. X-ray diffraction characterization

Figure 1 shows the room temperature XRD patterns of the as-sintered and quenched ceramics, as well as the CCTO powders (CCTO-M) prepared by molten salt method. We can see that the diffraction peaks of the three samples are well matched with data of the standard JCPDS card of pure CCTO (number: 75-2188), indicating that all the three samples are of single-phase. The diffraction peaks at 34.29°, 49.27°, 61.40°, 72.25°, and 82.47° correspond to the (220), (400), (422), (440), and (620) crystal planes of CCTO, respectively. These relatively sharp and narrow diffraction peaks indicate that the sample has high crystallinity and phase purity.[33] The peak width of the quenched CCTO is slightly lower than that of the as-sintered CCTO, which may be caused by the decrease in crystallinity of the sample and the generation of defects under high pressure.

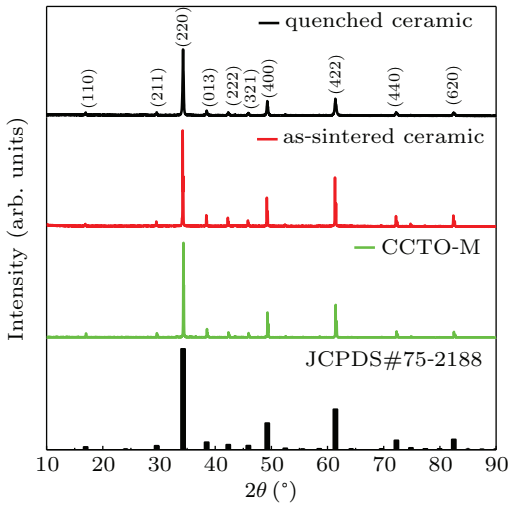


Fig. 1. X-ray diffraction patterns for samples of quenched ceramic, as-sintered ceramic, and CCTO-M.

3.2. Microscopic characterization

Figure 2 shows the SEM images for some prepared ceramics. We can see that both the as-sintered ceramic (see Figs. 2(a) and 2(b)) and quenched ceramic (see Figs. 2(c) and 2(d)) become dense with uneven grain size increasing. The grain size of the as-sintered ceramic increases from 5 μm to 30 μm, and the average grain size of quenched ceramic is about 20 μm. The grain shapes of both samples are irregular. Comparing with the as-sintered ceramics, the grain surface of the quenched ceramic is obviously rough, and the grain boundary is blured but has no holes, which may be attributed to the high pressure compression. Such topographic characteristics suggest that there may be more defects in quenched

samples, which is consistent with the band width in the XRD results. Figures 3(a) and 3(b) show the SEM images of the CCTO powders prepared by molten salt method (CCTO-M). We can see that the particles are polyhedral with uneven sizes. The larger particle is about 3 μm in size, and the small one is about 300 nm in size. Usually the single CCTO particle prepared by molten salt method is monocrystalline.[34] The etchings and cracks on the surface of particle may be caused by the electrostatic absorption of the salt ions on CCTO particle surface.[35] Owing to the growth environment in molten salt, the CCTO particle is easily oxygen deficient, with dual defects of oxygen vacancy and metal acceptor ions appearing.[34] Figure 3(c) shows the elemental composition image obtained by the energy dispersive spectroscopy (EDS), suggesting that the structure is of a pure phase, for it contains the peak of Ca, Cu, Ti, and O only.

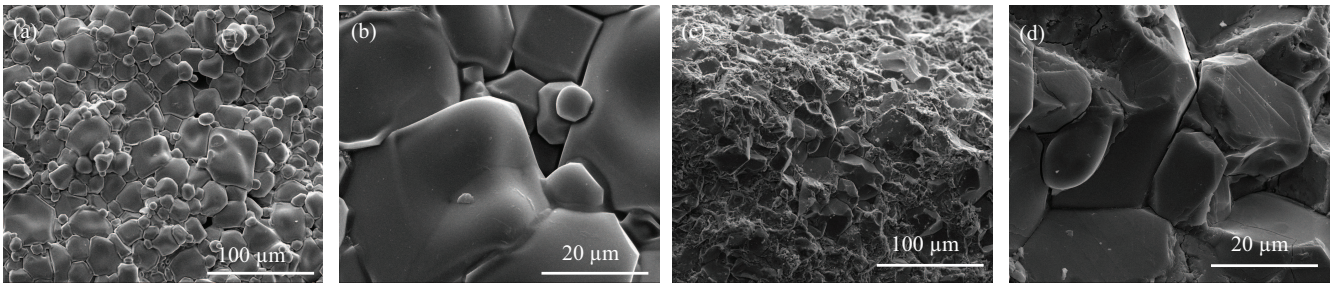


Fig. 2. SEM images of surface morphologies for ((a), (b)) as-sintered ceramic sample and ((c), (d)) quenched ceramic sample.

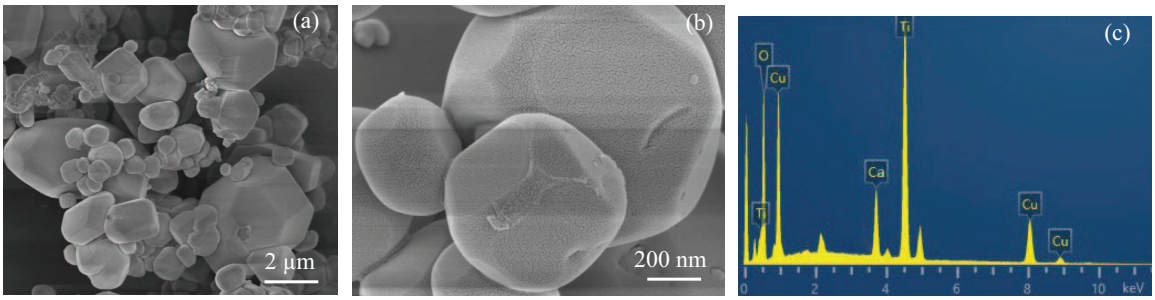


Fig. 3. ((a), (b)) SEM images of surface morphologies and (c) energy dispersive spectrum of CCTO-M sample.

3.3. X-ray photoelectron spectrum analysis

In order to further check the impurity or defect states, we perform the XPS analyses in detail for all the samples. Figure 4 shows the full range XPS spectra of all the samples prepared. We see that all samples show the peak of Ca, Ti, Cu, O ions, without any obvious distinctions appearing. The binding energy of the C 1s peak at 284.8 eV is used to calibrate the binding energy. Figure 5(a) shows the high-resolution XPS spectra of the Ca 2p peak. The two symmetrical peaks at 346.5 eV and 350.0 eV with spin–orbit splitting energy of 3.5 eV, represent the Ca $2p_{3/2}$ peak and Ca $2p_{1/2}$ peak, respectively, which correspond to Ca^{2+}. None of the four samples shows any obvious distinction on Ca^{2+}. Figure 5(b) shows the high-resolution XPS spectra of the Cu 2p peak for all samples. The Cu $2p_{3/2}$ peak and Cu $2p_{1/2}$ peak are at 933.9 eV and 953.7 eV, respectively, and the spin–orbit splitting energy is 19.8 eV. Two satellite peaks at 942.1 eV and 961.9 eV can also be observed, which are the characteristic of Cu^{2+}.[34] In order to determine the valence states of Cu ions, we fit the experimental data by the binding energy of Cu^{1+} ion and Cu^{2+} ion. As shown in Fig. 5(b), the black lines are the experimental data, the red lines denote the fitted data, and the peaks related to Cu^{1+} and Cu^{2+} are fitted with the lines in different colors. By setting the binding energy of 932.1 eV for Cu^{1+} and 934.9 eV for Cu^{2+} in Cu $2p_{3/2}$ peak, and of 951.9 eV for Cu^{1+} and 953.9 eV for Cu^{2+} in Cu $2p_{1/2}$ peak, the experiment curves for all the samples can be fitted quite well, indicating the Cu^{1+} acceptor existing in all the samples. In Table 1 we list the content of Cu^{1+} in detail.

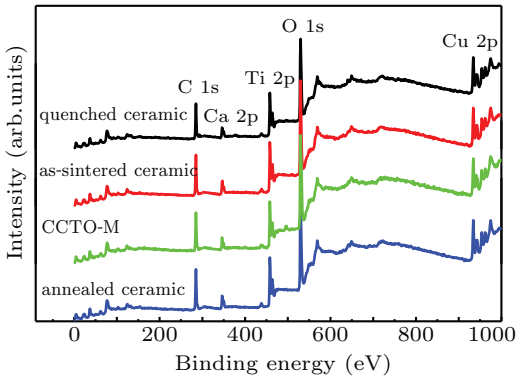


Fig. 4. Full range XPS spectrum for quenched ceramic, as-sintered ceramic, annealed ceramic, and CCTO-M samples.

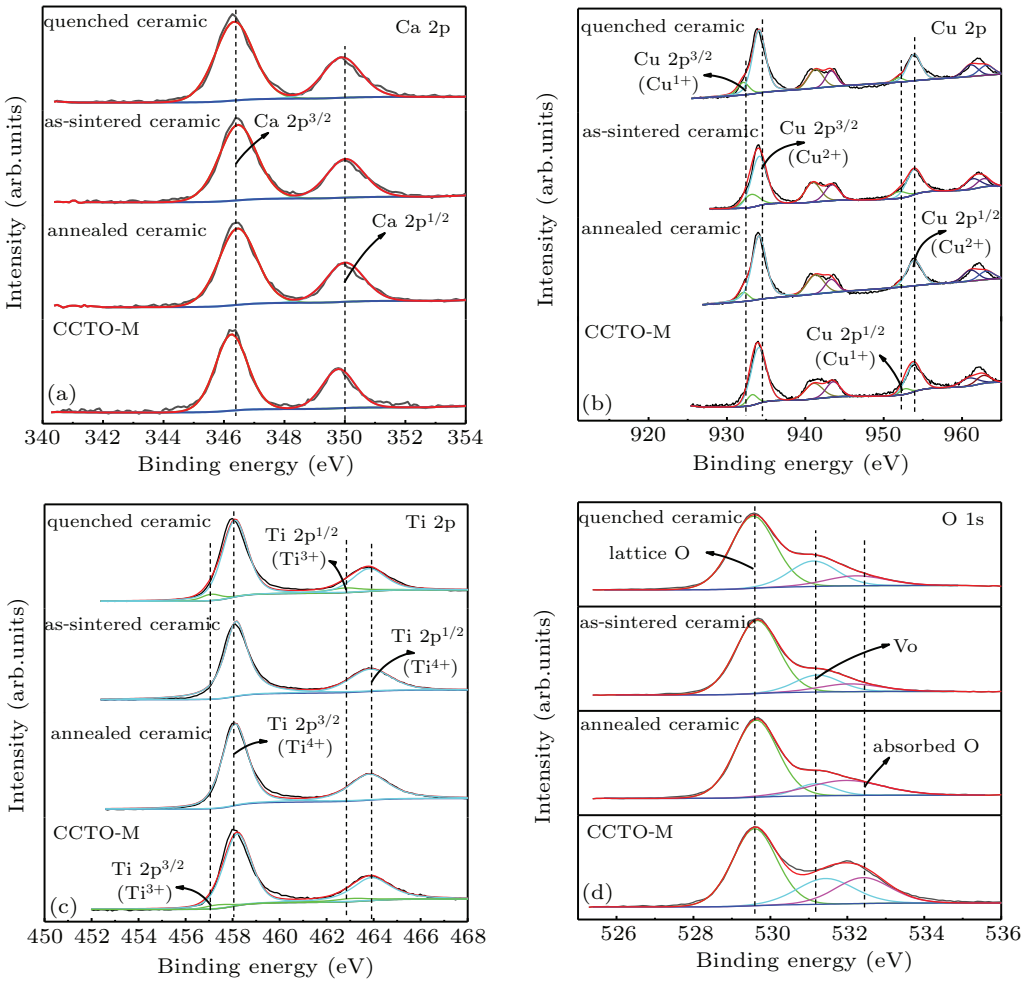


Fig. 5. High-resolution XPS spectrum of (a) Ca 2p, (b) Cu 2p, (c) Ti 2p, and (d) O 1s for s quenched ceramic, as-sintered ceramic, annealed ceramic, and CCTO-M samples.

Table 1. Ratio of Cu^{1+} to Cu^{2+}, $Ti^{3+}$to Ti^{4+}, and lattice oxygen to oxygen vacancy to absorbed oxygen for (a) quenched ceramic, (b) as-sintered ceramic, (c) annealed ceramic, and (d) CCTO-M samples.

	Cu		Ti		O		
	Atomic ratio (%)		Atomic ratio (%)		Atomic ratio (%)		
	Cu^{1+}	Cu^{2+}	Ti^{3+}	Ti^{4+}	Lattice O	V_O	Absorbed O
(a)	12.3	87.7	10.7	89.3	63.7	24.2	12.1
(b)	16.2	83.8	0	100	71.9	17.3	10.8
(c)	11.1	88.9	0	100	69.9	12.6	17.5
(d)	11.6	88.4	7.4	92.6	56.1	21.2	22.7

The Ti 2p high-resolution XPS spectrum is shown in Fig. 5(c). Owing to the $2p_{3/2}$ and $2p_{1/2}$ of the Ti^{4+} state, all samples show obvious peaks at 458.1 eV and 463.8 eV, respectively.[36] Only the peaks of quenched ceramic and CCTO-M can be deconvolved into two $2p_{3/2}$ peaks (457.1 eV and 458.1 eV) and two $2p_{1/2}$ peaks (462.8 eV and 463.8 eV). Two peaks on the higher-energy side 458.1 eV and 463.8 eV are attributed to Ti^{4+}, while the two peaks on the lower-energy side 457.1 eV and 462.8 eV are attributed to Ti^{3+}. However, for the annealed ceramic, no Ti^{3+} peak can be observed, indicating that the most of Ti^{3+} ions in quenched samples have been reoxidized in air.

The presence of low valence Cu^{1+} and Ti^{3+} suggests that the samples are oxygen deficient with oxygen vacancies needing charge compensation. Figure 5(d) shows the high-resolution XPS spectrum of O 1s. We see an obvious broad peak at 529.7 eV which extends to the high binding energy, suggesting that O atoms in the samples are in different chemical states. The O 1s peaks of all samples are deconvolved into three Gaussian peaks. The lowest binding energy peak at 529.5 eV is related to the state of O^{2-} in the crystal lattice (lattice oxygen). The peak with binding energy of 531.2 eV can be attributed to oxygen vacancies (V_O) formed by the escape of lattice oxygen in the sample synthesis process, and the in-

tensity of this peak is proportional to the oxygen vacancy concentration. The peak at 532.4 eV is caused by adsorbing H_2O, O_2 or other pollutants (absorbed oxygen).[37] We find that for the annealed ceramic (based on the quenched ceramic), the oxygen vacancy content is significantly reduced, suggesting that Cu^{1+} and Ti^{3+} reoxidize in the annealing process. Based on the fitting results of the XPS spectra, the ratio of Cu^{1+} to Cu^{2+}, Ti^{3+} to Ti^{4+}, and lattice oxygen to oxygen vacancies to absorbed oxygen in the sample are calculated, and the results are shown in Table 1. We see that both the quenched ceramic and CCTO-M have higher oxygen vacancy content and higher Ti^{3+} ions content as well.

3.4. Magnetism of CCTO

Figure 6 shows the temperature-dependent magnetic moment (M–T) curves recorded in the field cooling (FC) and zero field cooling (ZFC) states in a magnetic field of 20 Oe. All samples show a maximum value near the temperature 25 K, which is referred to Neel temperature (T_N), in a good consistent with the value reported previously.[26,38] The ZFC and FC magnetization curves are not separated from each other obviously in the entire measurement temperature range, and have good reversibility, which excludes the existence of any spin glass state. The Cu^{2+} ion in CCTO has an unusual triple degenerate t_{2g} state, resulting in a strong coupling between the crystal structure and the magnetic structure.[39,40] By calculations Shimakawa showed that the Ti 3d band in CCTO strongly hybridizes with the O 2p and Cu 3d orbitals near the Fermi level and participates in the exchange interaction.[40] Specifically, an indirect exchange between the magnetic moments of Cu^{2+} ions is achieved through O^{2-} ions and Ti^{4+} ions with a triple-degraded t_{2g} ground state, or through Ti^{4+} and O^{2-} ions with five undegraded ground states,[41] leading to an antiferromagnetic superexchange interaction through the path of Cu–O–Ti–O–Cu.

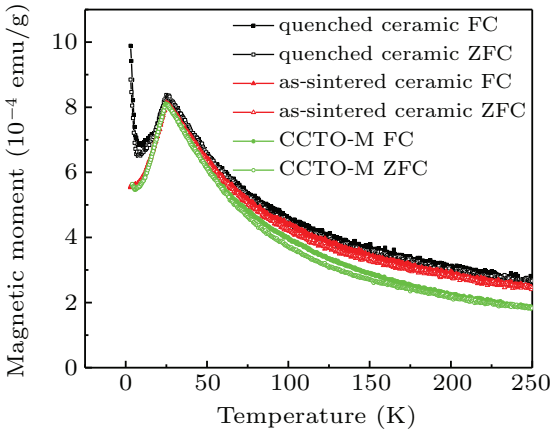


Fig. 6. Temperature-dependent magnetization curves in field-cooled (FC) and zero-field cooled (ZFC) modes recorded at applied magnetic field of 20 Oe for quenched ceramic, as-sintered ceramic, and CCTO-M samples.

However, in the thermomagnetic curves of quenched ceramic and CCTO-M powders, there appear low-temperature Curie tails below 9 K and 6.5 K, respectively, as shown in Fig. 6. The further measurement of the magnetization (in units emu/g) *versus* applied magnetic field (in unit Oe) curves suggest that there is a feature of weak ferromagnetic behavior in quenched ceramic and CCTO-M, which behave as the hysteresis loops, each with an unsaturated and small remanence as shown in Figs. 7(a) and 7(c), indicating a coexistence of antiferromagnetic and weak ferromagnetism.[42] According to the local density approximation, Li *et al*. reported a metastable FM state in CCTO by means of the spin-polarized moment method and the fixed-spin-moment method, indicating an AFM–FM transition.[4] The AFM state is calculated to be 84 meV lower in energy than the FM state by the generalized gradient approximation (GGA). Shimakawa investigated the magnetic behaviors in $CaCu_3B_4O_{12}$ (B = Ge, Ti, and Sn) perovskite-like oxide based on the in-depth experimental and theoretical analysis.[40] Shimakawa thought that the involvement of Ti 3d orbitals caused antiferromagnetic superexchange interaction between the Cu^{2+} spins overcomes the ferromagnetic direct interaction. According to Shimakawa's experimental investigation of the ferromagnetic behavior in $CaCu_3(Ge_{1-x}Ti_x)_4O_{12}$ ($x < 0.4$) and $CaCu_3(Ti_{1-y}Sn_y)_4O_{12}$ ($y > 0.6$) we find that when the foreign ions doping on B site in CCTO exceeds 12 at.%, some direct-exchange interaction between Cu^{2+} spin will replace the antiferromagnetic superexchange interaction. Without doping, Raval *et al*. also found a Curie tail and a weak ferromagnetic loop at 5 K in pure CCTO polycrystal mechanically grinded for 16 h.[31] By doping only 0.25 at.%–1 at.% Co ions on Cu site, Wang *et al.* also found the weak ferromagnetism in $CaCu_{3-x}Co_xTi_4O_{12}$ (x = 0.05, 0.10, 0.20), with the coercivity values of 58.47, 106.40, and 146.93 Oe, respectively.[43] The XPS study shows that in $CaCu_{3-x}Co_xTi_4O_{12}$ (x = 0.05, 0.10, 0.20) there are mixed-valent metal ions of Cu^{1+}/Cu^{2+}, Ti^{3+}/Ti^{4+}, and Co^{3+}/Co^{2+}, as well as oxygen vacancies, and the content of acceptor Ti^{3+} ions increases with the doping content of x increasing.[43] In Table 2 listed are the composition, doping percentage, and the content of mixed-valent ions or oxygen vacancies mentioned in the CCTO samples with Curie tails or FM hysteresis loops yielded by different samples. In the temperature range where the Curie tails appeared in Refs. [28,41], though there is no mention of further investigation FM in the temperature range, we deduce that it may contain the FM phase. In Refs. [30,41,44], there is no mention of the mixed-valence ions' characterizations but the doping ions themselves are of mixed-valence. The list in Table 2 suggests that the FM phase can be obtained through different preparation processes or doping methods, which may produce oxygen vacancies by compensating for mixed-valence metal ions.

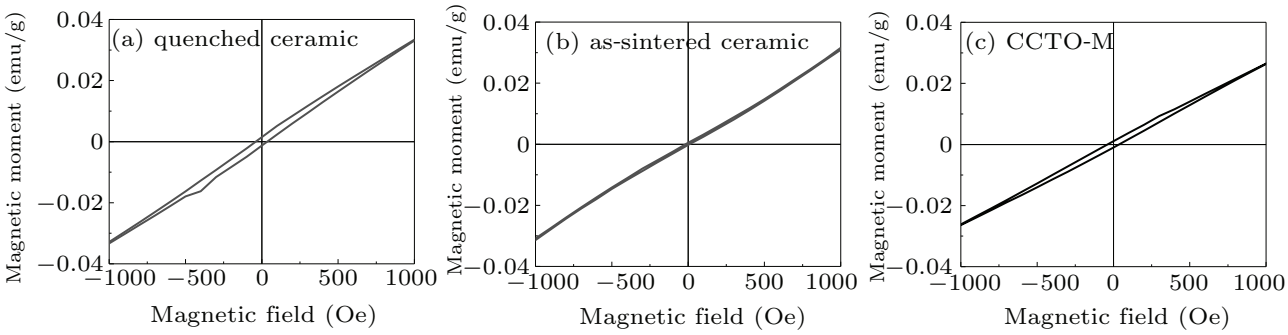


Fig. 7. Isothermal magnetization curves for (a) quenched ceramic, (b) as-sintered ceramic, and (c) CCTO-M samples recorded at 5 K.

The influence of oxygen vacancy on the magnetism has been investigated intensively in the dilute magnetic semiconductors with wide band gap.[33,45,46] Coey *et al.* proposed a bound magnetic polaron (BMP) model to explain the FM appearing in dilute oxides, where shallow donor electrons form BMPs that overlap to create a spin-split impurity band.[47] The long range indirect magnetic interaction between two magnetic polarons can be mediated by carriers in a spin-polarized band. The coupling between the cation and the donor electron is ferromagnetic when the 3d shell is less than half full.[47] The BMP model has been confirmed experimentally to play an important role in activating the FM characteristics in dilute oxides.[48,49] Oxygen vacancies appearing in these oxides may be occupied by a single electron, forming an F^+ center[50] and mediating the indirect FM interaction. It seems that for the Curie tail or FM loop to occur, we should consider not only the change of exchange interaction influenced by doping content, but also the contribution of defects such as mix-valent metal ions or oxygen vacancies caused by different preparation processes or dopings. In our situation, we do not dope CCTO with foreign ions, but different post processing indeed produces some defects, such as oxygen vacancy (V_O), metal ion acceptors Cu^{1+} and Ti^{3+}, as shown in Fig. 5 and Table 1. Note that Cu^{1+} and V_O exist in all the samples prepared, but Ti^{3+} ions exist only in quenched ceramic and CCTO-M powders which show the weak FM characteristics. For quenched ceramic and CCTO-M, their total atomic percentages of Ti^{3+} ions reach to 2.1 at.% and 1.5 at.%, and those of oxygen vacancies arrive at 14.5% and 12.7%, respectively, while for other samples without any obvious FM, we cannot obtain Ti^{3+} peak by fitting the XPS lines. In Wang *et al.*'s work, we also find that the coercivity increases with the content of Ti^{3+} increasing after Co doping.[43] These results suggest that the FM characteristic is strongly related to content of Ti^{3+} ions and the compensated oxygen vacancies.

Table 2. Compositions, doping content of CCTO (or doped) with Curie tail/FM.

Composition	Atomic percent of doping	Preparation methods	Curie tail	FM hysteresis loop	V_O, Cu^{1+}/Cu^{2+}, Ti^{3+}/Ti^{4+}
$CaCu_3Ti_4O_{12}$ (single crystal)[28]	0	traveling-solvent floating zone method	Yes	No mention	Yes
$CaCu_3Ti_4O_{12}$ (Ar anneal)[28]	0	solid state reaction	Yes	No mention	Yes
$CaCu_3Ti_4O_{12}$[41]	0 1 at.% Mn 0.5 at.% Fe 0.5 at.% Ni	organic gel-assisted citrate synthesis	Yes	No mention	No mention
$CaCu_3Ti_{4-x}Co_xO_{12}$ ($x = 0.2$)[32]	1 at.% Co	solid state reaction	Yes	Yes	Yes
$CaCu_{3-x}Co_xTi_4O_{12}$ ($x = 0.05$, 0.1, 0.2)[43]	0.25 at.% ∼ 1 at.% Co	solid state reaction	Yes	Yes	Yes
$CaCu_{3-x}Ti_{4-x}Fe_{2x}O_{12}$ ($x = 0.5$, 0.7)[30]	5 at.%∼7 at.% Fe	solid state reaction	Yes	Yes	No mention
$CaCu_3Ti_4O_{12}$[31]	0	mechanical grinding for16 hours	Yes	Yes	Yes
$Ca_{1+x}Cu_{3-x}Ti_4O_{12}$ ($x = 0.1$, 0.2)[44]	0.5 at.%∼1 at.% Ca	solid state reaction	Yes	Yes	No mention

The ferromagnetism observed in quenched ceramic and CCTO-M which have more oxygen vacancies and Ti^{3+} ions can be explained by using the bound magnetopolaron (BMP) model. One trapped electron in oxygen vacancy may occupy the nearby Ti 3d orbitals, inducing adjacent Ti^{4+} ions to transform into magnetic Ti^{3+} ions, forming a BMP with a pattern of Ti^{3+}–V_O defect complex, which will produce a localized effective magnetic field. The magnetic interaction between BMP spin and neighboring Cu^{2+} spin may be ferromagnetic. The macroscopical ferromagnetic ordering is caused when the cluster of such a BMP–Cu^{2+} ferromagnetic coupling forms. The concentration of magnetopolarons is positively correlated with oxygen vacancies. In an annealed ceramic, Ti^{3+} ions are oxidized and the concentration of oxygen vacancies decreases, and the BMP formed by Ti^{3+}–V_O defect complex disappears, thereby losing ferromagnetic coupling as shown in Fig. 8. It is easy to rule out the influence of Cu^{1+} ions on the ferromagnetism of CCTO, for the non-magnetic Cu^{1+} ($3d^{10}$) ions have completely filled 3d orbitals and have no contribution to ferromagnetism.[31]

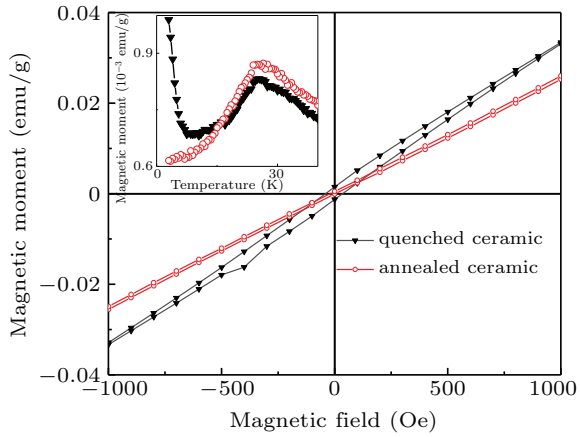


Fig. 8. Hysteresis loop of the quenched sample before and after annealing at 5 K, with inset showing temperature-dependent magnetization in field cooling mode at applied magnetic field 20 Oe.

4. Conclusions

In this work, we have studied the magnetic properties of different prepared CCTO samples in order to investigate the relation between the magnetism and defect in CCTO. In the CCTO ceramics quenched at a high pressure, and the CCTO powders made by molten salt method, we find the weak ferromagnetism below the Neel temperature. According to the detailed analysis and fitting of XPS spectra, we find that Ti^{3+} ions and a large number of oxygen vacancies appear in the samples that show ferromagnetic behaviors, which can disappear when the sample is postannealed. We think the BMP formed by Ti^{3+}–V_O defect complex is responsible for the ferromagnetism. In our previous work, we also examined the contribution of the defect complex to the large permittivity in CCTO. According to the results above, we believe that the FM phase can be obtained by increasing the content of Ti^{3+}–V_O defect complexes in CCTO through different preparation processes, which may make CCTO a promising material in magnetoelectric component.

References

[1] Subramanian M, Li D, Duan N, Reisner B and Sleight A 2000 *J. Solid State Chem.* **151** 323
[2] Homes C, Vogt T, Shapiro S, Wakimoto S and Ramirez A 2001 *Science* **293** 673
[3] Cheng P, Cao Z, Zhou M, Wang Q, Li S and Li J 2019 *Ceram. Int.* **45** 15320
[4] Li G L, Yin Z and Zhang M S 2005 *Phys. Lett. A* **344** 238
[5] Gaâbel F, Khlifi M, Hamdaoui N, Beji L, Taibi K and Dhahri J 2019 *J. Mater. Sci.-Mater. Electron.* **30** 148231
[6] Kadyrova N, Mel'nikova N, Ustinova I and Zainulin Y G 2016 *Inorg. Mater.* **52** 1051
[7] Fang T T and Mei L T 2007 *J. Am. Ceram. Soc.* **90** 638
[8] Ni L and Chen X M 2007 *Appl. Phys. Lett.* **91** 122905
[9] Lunkenheimer P, Fichtl R, Ebbinghaus S G and Loidl A 2004 *Phys. Rev. B* **70** 172102
[10] Sinclair D C, Adams T B, Morrison F D and West A R 2002 *Appl. Phys. Lett.* **80** 2153
[11] Ma Y, Liu J, Gao C, Mei W, White A D and Rasty J 2006 *Appl. Phys. Lett.* **88** 191903
[12] Jumpatam J, Putasaeng B, Yamwong T, Thongbai P and Maensiri S 2013 *Ceram. Int.* **39** 1057
[13] Jesurani S, Kanagesan S, Hashim M and Ismail I 2013 *J. Alloys Compd.* **551** 456
[14] Thongbai P, Jumpatam J, Yamwong T and Maensiri S 2012 *J. Eur. Ceram. Soc.* **32** 2423
[15] Li M, Chen X, Zhang D, Liu Q and Li C 2015 *Ceram. Int.* **41** 14854
[16] Hu W, Liu Y, Withers R L, Frankcombe T J, Norén L, Snashall A, Kitchin M, Smith P, Gong B and Chen H 2013 *Nat. Mater.* **12** 821
[17] Luo X, Bärner K, Zhang Y, Gao T, Yang C and Liu Y 2018 *Ceram. Int.* **44** 12007
[18] Luo X, Zhang Y, Xu D, Chen S, Wang Y, Chai Y, Liu Y, Tang S, Yang C and Bärner K 2019 *Ceram. Int.* **45** 12994
[19] Liu Y, Feng S, Li Z, Zhang L, Wang G, Chen W, Wang T and Zhong W 2016 *RSC Adv.* **6** 57013
[20] Wang X, Song Y, Tao L, Feng J, Sui Y, Tang J, Song B, Wang Y, Wang Y and Zhang Y 2014 *Appl. Phys. Lett.* **105** 262402
[21] Singhal R, Kumar S, Kumari P, Xing Y and Saitovitch E 2011 *Appl. Phys. Lett.* **98** 092510
[22] Sarin N, Mishra M, Gupta G, Arora M and Luthra V 2018 *Physica Status Solidi (b)* **255** 1700683
[23] Parras M, Varela A, Corteés-Gil R, Boulahya K, Hernando A and González-Calbet J M 2013 *J. Phys. Chem. Lett.* **4** 2171
[24] Song Y, Wang X, Tao L, Song B, Zhang L, Zhang Y, Sui Y, Liu Z, Tang J and Han X 2017 *J. Alloys Compd.* **694** 929
[25] Bapna K, Choudhary R, Pandey S, Phase D, Sharma S and Knobel M 2011 *Appl. Phys. Lett.* **99** 112502
[26] Kim Y, Wakimoto S, Shapiro S, Gehring P and Ramirez A 2002 *Solid State Commun.* **121** 625
[27] Koitzsch A, Blumberg G, Gozar A, Dennis B, Ramirez A, Trebst S and Wakimoto S 2002 *Phys. Rev. B* **65** 052406
[28] Pires M, Israel C, Iwamoto W, Urbano R, Agüero O, Torriani I, Rettori C, Pagliuso P, Walmsley L and Le Z 2006 *Phys. Rev. B* **73** 224404
[29] Fernandez J F, Leret P, Romero J J, De Frutos J, De La Rubia Má, Martín-González M S, Costa-Krämer J L, Fierro J L G, Quesada A and García M 2009 *J. Am. Ceram. Soc.* **92** 2311
[30] Pansara P, Raval P, Vasoya N, Dolia S and Modi K 2018 *PCCP* **20** 1914
[31] Raval P, Pansara P, Makadiya A, Vasoya N, Dolia S and Modi K 2018 *Ceram. Int.* **44** 17667
[32] Mu C, Song Y, Wang H and Wang X 2015 *J. Appl. Phys.* **117** 17B723

[33] Shi J, Chang Y, Tang Y, Wang X, Yao W, Yue Z, Minhas B and Cao J 2020 *Ceram. Int.* **46** 5360
[34] Maity S, Samanta M, Sen A and Chattopadhyay K K 2019 *J. Solid State Chem.* **269** 600
[35] Hailili R, Wang Z Q, Li Y, Wang Y, Sharma V K, Gong X Q and Wang C 2018 *Appl. Catal B-Environ.* **221** 422
[36] Ghosh S and Nambissan P 2019 *J. Solid State Chem.* **275** 174
[37] Salameh B, Alsmadi A and Shatnawi M 2020 *J. Alloys Compd.* **835** 155287
[38] Mozzati M C, Azzoni C B, Capsoni D, Bini M and Massarotti V 2003 *J. Phys.: Condens. Matter* **15** 7365
[39] Grubbs R K, Venturini E, Clem P, Richardson J, Tuttle B and Samara G 2005 *Phys. Rev. B* **72** 104111
[40] Shimakawa Y 2008 *Inorg. Chem.* **47** 8562
[41] Krohns S, Lu J, Lunkenheimer P, Brize V, Autret-Lambert C, Gervais M, Gervais F, Bouree F, Porcher F and Loidl A 2009 *Eur. Phys. J. B* **72** 173
[42] Wang B, Gong L, Wang S, Zhou Z and Ma G 2015 *Int. J. Appl. Ceram. Tec.* **12** 157
[43] Wang J, Lu Z, Deng T, Zhong C and Chen Z 2018 *J. Eur. Ceram. Soc.* **38** 3505
[44] Barad D, Meshiya U, Joshi N, Mange P, Raval P, Kumar S, Singhal R, Dolia S and Modi K 2020 *Solid State Sci.* **99** 106070
[45] Wang Z Z, Zhang J M, Huang Z G and Lin W X 2011 *Chin. Phys. B* **20** 027103
[46] Ding B F and Zhou S Q 2011 *Chin. Phys. B* **20** 127701
[47] Coey J, Venkatesan M and Fitzgerald C 2005 *Nat. Mater.* **4** 173
[48] Khare N, Kappers M J, Wei M, Blamire M G and MacManus-Driscoll J L 2006 *Adv. Mater.* **18** 1449
[49] Griffin K, Pakhomov A, Wang C, Heald S and Krishnan K M 2005 *Phys. Rev. Lett.* **94** 157204
[50] Singhal R, Kumar S, Kumari P, Xing Y and Saitovitch E 2011 *Appl. Phys. Lett.* **98** 092510